Improved lithology prediction in channelized reservoirs by integrating stratigraphic forward modelling: towards improved model calibration in a case study of the Holocene Rhine-

Improved lithology prediction in channelized reservoirs by integrating stratigraphic forward modelling: towards improved model calibration in a case study of the Holocene Rhine-Meuse fluvio-deltaic system*

Costanzo Peter [a,1] costanzo.peter@polito.it (Corresponding author)
Eloisa Salina Borello [a,2] eloisa.salinaborello@polito.it
Rory A.F. Dalman [b,3] rory.dalman@tno.nl
Pantelis Karamitopoulos [c,4] pkaramitopoulos@gmail.com
Freek Busschers [b,5] freek.busschers @tno.nl
Quinto Sacchi [d,6] quinto.sacchi@dream-top.com
Francesca Verga [a,7] francesca.verga@polito.it

[a] Politecnico di Torino, Engineering Faculty, Department of Environment, Land and Infrastructure Engineering, Torino, Italy
[b] TNO, Geological Survey of the Netherlands, Utrecht, the Netherlands
[c] Delft University of Technology, Department of Geoscience and Engineering, Delft, the Netherlands
[d] Dream s.r.l., Dedicated Reservoir Engineering and Management, Turin, Italy

Abstract

Stratigraphic forward modelling (SFM) provide the means to produce geologically coherent and realistic models. In this paper, we demonstrate the possibility of matching lithological variability simulated with a basin-scale advection-diffusion SFM to a data-rich real-world setting, i.e. the Holocene Rhine-Meuse fluvio-deltaic system in the Netherlands. SFM model calibration to real-world data in general has proven non-trivial. This study focuses on a novel inversion process constrained by the top surface and the sand proportion observed at specific pseudo-wells in the study area. Goodness-of-fit expressed by a new fitness function, gives the error calculated as the average of two calibration

*
1 Built the GeoTOP model in Petrel, carried out the basin simulations, analyzed and interpreted the results, co-wrote and reviewed the manuscript
2 Wrote and implemented the optimization algorithm in MATLAB, analyzed and interpreted the results, co-wrote and reviewed the manuscript
3 Initiated the study, support for SimClast code, provided the necessary data, analyzed and interpreted the results, co-wrote and reviewed the manuscript
4 Support for SimClast code, analyzed and interpreted the results, co-wrote and reviewed the manuscript
5 Provided the necessary data, advisor and reviewed the paper
6 Advisor
7 Advisor and reviewed the paper

constraints. Computational efficiency was increased significantly by implementing a new optimization process in two hierarchical steps: a) optimization in terms of sediment load and discharge, which are the most influential parameters having the largest uncertainty and b) optimization with respect to the remaining uncertain parameters, these being sediment transport parameters. The calibration process described allows for the most optimal combination of achieving acceptable levels of goodness-of-fit, feasible runtimes and multiple (non-unique) solutions to obtain synthetic stratigraphic output best matching real-world datasets.

By removing model realizations which are geologically unrealistic, calibrated SFM models provide a multiscale stratigraphic framework for reconstructing static models of reservoirs which are consistent with the palaeogeographic layout, basin-fill history and external drivers (e.g. sea level, sediment supply). The static reservoir models that are matched with highest certainty therefore contain the highest geological realism and may be used to improve deep subsurface reservoir or aquifer property prediction.

The new methodology was applied to the well-established Holocene Rhine-Meuse dataset which allows a rigorous testing of the optimization and the calibrated SFM allows investigation of controls of the Holocene development on the sedimentary system.

Keywords: Stratigraphic forward modeling; basin modeling; fluvio-deltaic; inverse algorithm; model calibration

Nomenclature

SFM: Stratigraphic forward modeling

sl: Sediment load

q: Discharge

$e_{s:}$ Exponent of slope

$c_{s:}$ Stream transport coefficient

NA: Neighborhood algorithm

n_s: Initial population

n_{dim}: Number of uncertain parameters

55 max_H: Maximum reservoir thickness

56 N: binary parameter

57 d.o.f.: degree of freedom

58

59 **1. Introduction**

60 Reservoirs with complex sedimentary heterogeneities such as low net-to-gross channelized deposits
61 hold significant amounts of energy resources worldwide. Despite locally good reservoir quality, the
62 estimation of reservoir properties in these heterogeneous deposits remains highly uncertain. The
63 inherent heterogeneities in these deposits necessitate geological reservoir models, which are typically
64 based on stochastic geometric and interpolation methods (Deutsch, 2002). Such methods generate
65 solutions which are locally optimal, capturing the overall setting but are not constrained by the large-
66 scale geological setting of the reservoir (Weltje et al., 2013) nor include processes associated with
67 sediment dispersal and deposition. Stratigraphic forward models (SFMs), that combine topographic
68 diffusion and advective transport equations, are well suited for investigating the morphodynamic and
69 resulting stratigraphic evolution of sediment dispersal systems over a wide range of spatial and
70 temporal scales (Granjeon and Joseph, 1999; Paola, 2000; Meijer, 2002; Hajek and Wolinsky, 2012).
71 Using SFM's inherent holistic approach and geological results, they provide attractive tools for
72 incorporating basin-scale information at the reservoir scale through the conditioning of geological
73 data in a variety of ways (Cross and Lessemger, 1999; Wijns et al., 2004; Imhof and Sharma, 2006;
74 Charvin et al., 2009; Falivene et al., 2014).
75 Efficiency in matching the data is essential because it determines the applicability of SFMs in real
76 field cases (Bertonello et al., 2013). Karssenberg et al. (2001, 2007) demonstrated the possibility of
77 conditioning SFMs to well data using a simple 3D alluvial architecture model characterized by a
78 single channel belt moving by avulsion over an aggrading floodplain. Sacchi et al. (2015, 2016)
79 implemented the method proposed by Weltje et al. (2013) for conditioning the stratigraphic output
80 derived from SimClast (Dalman and Weltje, 2008, 2012), a basin-scale advection-diffusion model of
81 fluvio-deltaic systems, in which the channels are represented by sub-grid elements. This SFM
82 provides a more efficient sediment transport algorithm for reproducing channelized flow as opposed

to conventional linear diffusion models (Meijer, 2002; Dalman and Weltje, 2008; Falivene et al., 2014; Karamitopoulos et al., 2014; Sacchi et al., 2016).

This workflow has been shown to work in a synthetic setting. The simulated channel occurrences were: a) fitted (conditioned) to synthetic seismic and local well data and b) integrated as soft constraints in geostatistical reservoir modelling. The static reservoir models that were constrained to maintain the quantitative coherence with the synthetic large-scale geological setting improved predictive power relative to the models using local well data only.

In this case study, we conditioned SimClast (output/channel occurrences) to a data-rich real-world setting, i.e. the Holocene Rhine-Meuse fluvio-deltaic system. The calibration dataset consists of detailed lithological information obtained from GeoTOP, a high-resolution 3D voxel model that captures the distribution of channel bodies and overbank fines of the fluvial-deltaic deposits in the shallow subsurface down to 50 m below mean sea level (Stafleu et al., 2011; 2012; Van der Meulen et al., 2013; Maljers et al., 2015: Stafleu and Dubelaar, 2016; Stafleu and Busschers 2017).

The applicability of a new workflow is demonstrated to a real-world setting through the implementation of a hierarchical optimization approach. This approach significantly differs from the one proposed by Sacchi et al. (2015, 2016), which adopted a less efficient Quasi-Monte Carlo approach with systematic sampling to explore the SFM parameter space. In fact, matching the SFM output to a real-world dataset requires a highly complex suite of parameters and calibration constraints compared to synthetic datasets. Therefore, a more efficient matching routine was required to minimize the number of runs to find the most optimal solution or solutions. Moreover, Sacchi et al. (2015) used a well calibration fitness functions based on well tops and lithological logs which turned out to be less effective for the inversion process. Therefore, in this study the well calibration function is based on the average net-to-gross values at wells to manage the scale difference between well (meter scale) and SFM (kilometer grid scale) information, which can be problematic when calibrating well data (Sacchi et al., 2016), This is in line with Falivene et al (2014), who observed that the representativeness problem could be mitigated by averaging over relatively large intervals.

By using the data-rich Holocene-Rhine Meuse GeoTOP model the robustness of the workflow is illustrated and expanded where necessary. The predictive capabilities by incorporating synthetic

stratigraphy created by the SFM through the sedimentary processes are shown. Lessons learned may be taken to future applications in deeper subsurface examples for accurate resource estimation. In addition to testing hypotheses on the controlling parameters of the sedimentary system in question, the matched/calibrated basin-scale model allows further use in constraining static models of channelized reservoirs.

2. Method

The proposed methodology may be summarized as follows (Figure 1):

- Pre-processing
  - ✓ Characterization of the reference case: Holocene Rhine-Meuse fluvio-deltaic system
  - ✓ Definition of the constraints used for the calibration process
  - ✓ Sensitivity analysis to extrapolate the range of the input parameters used for SFM
- Inversion process for SFM calibration
  - ✓ Stratigraphic forward modeling using SimClast
  - ✓ Application of the Neighborhood Algorithm to explore the domain of the unknown input parameters of SFM
- Result analysis
  - ✓ Comparison between the calibrated models from SimClast and the reference GeoTOP model

Our approach builds on the workflow proposed by Sacchi et al. (2015, 2016), but improves the methodology for both the definition of the fitness function expressing the calibration constraints and in the algorithm which explores the parameter space for optimal model calibration. Each step is described extensively in the following sections.

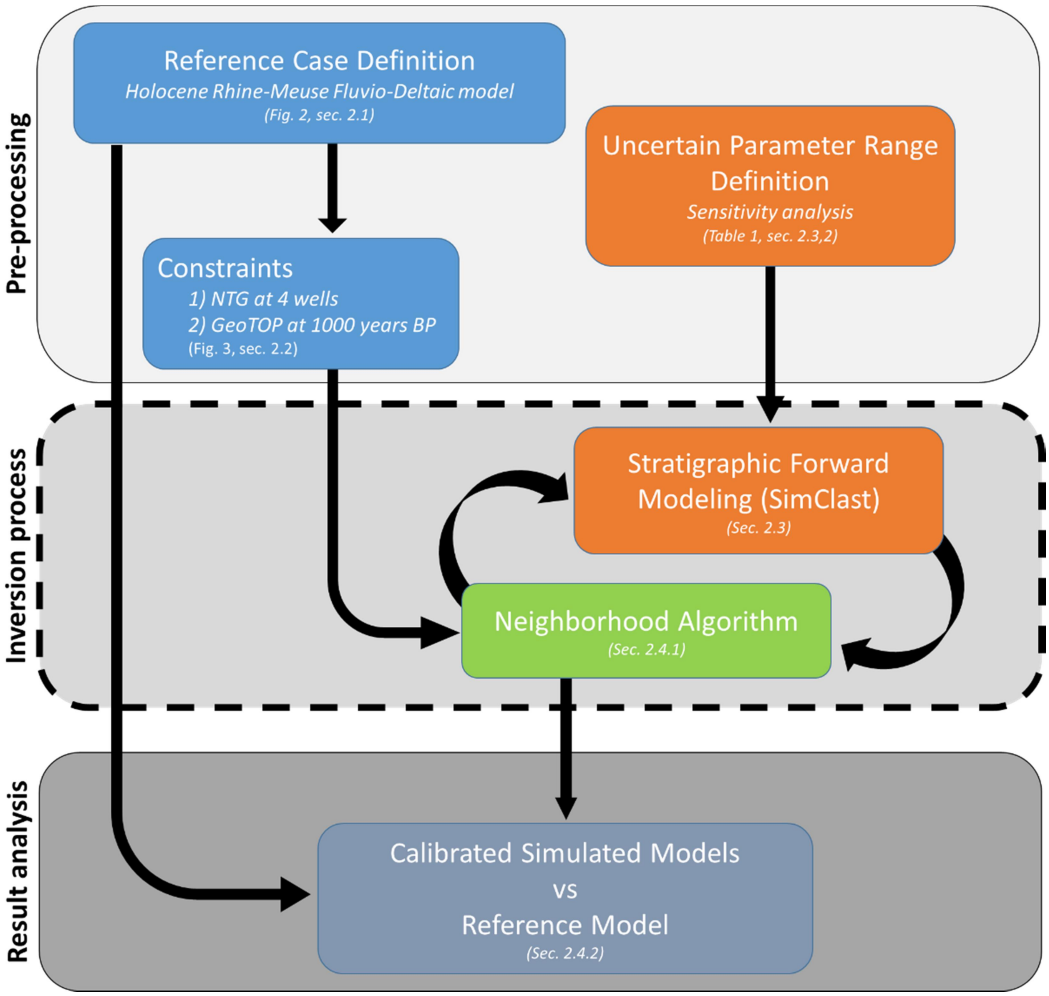

Figure 1: Stratigraphic Forward Model calibration workflow. The dashed box indicates the inversion stage represented in fig. 6.

2.1 Holocene Rhine-Meuse dataset

TNO-Geological Survey of the Netherlands systematically produces detailed 3D geological models of the Dutch subsurface (Van der Meulen et al., 2013). One of these models is the voxel model GeoTOP, which describes the geometry of the shallow subsurface to a maximum depth of 50 m below mean sea level (Stafleu et al., 2011; 2012; Van der Meulen et al., 2013; Maljers et al., 2015: Stafleu and Dubelaar, 2016; Stafleu and Busschers 2017). The model is freely available online from the Survey's web portal (www.dinoloket.nl/en). A major component of this static model are the Holocene Rhine-

Meuse fluvial deposits in the central part of the Netherlands (figure 2a). These fluvial sediments were deposited during the Holocene sea level rise, which started in the western part of the area at ~9000 years BP, allowing base level rise and a complex of sand rich fluvial channel belt systems encased in floodplain fines to be deposited. The channel belt positions in the GeoTOP model were taken from the channel belt maps of Utrecht University (Berendsen and Stouthamer, 2001; Cohen and Stouthamer, 2012). Base-level rise made that the tops of the younger channel belts occur at shallower depths. Controlling parameters such as sea-level (Hijma and Cohen, 2010) and discharge/sediment rates (Erkens et al., 2006; Koster et al., 2016) have been well studied and allow an estimate for the boundary conditions to be made for the SFM.

This high-resolution 3D model has a grid discretization of 100 x 100 x 0.5 m and each voxel contains subsurface information, including estimates of lithostratigraphy and lithology. The grid discretization adopted, coupled with the very high borehole data coverage, allows GeoTOP to be used as a reference scenario due to its accurate representation of the channel body geometries and associated spatial lithological heterogeneity.

In the present study, the focus is on the, non-anthropogenically influenced, Holocene (9000-1000 BP) fluvial deposits of the Zuid-Holland, Utrecht and Gelderland region, in the central part of the Netherlands' subsurface. The 1000 year timeframe was chosen as younger deposits are influenced heavily by anthropogenic dyke, dam construction and land reclamation. This region extends over approximately 80 by 145 km and mainly consists of a complex fluvial channel system subdivided into five distinctive Holocene channel belts deposits, each identified by a unique code number. The channel belt complexes are classified from younger (shallower) to older (deeper): AEC, BEC, CEC, DEC, EEC. (Figure 2a).

2.2 Definition of the calibration constraints

Two calibration constraints were extracted from the GeoTOP model: (1) the top surface, analogous to a 3D surface derived from seismic interpretation and time-depth conversion, covering the area influenced only by fluvial and alluvial processes in the Rhine-Meuse delta; (2) the net-to-gross values at four synthetic wells, arbitrarily located in order to uniformly investigate a hypothetical reservoir

area. The base surface was also used as an input constraint for the SFM simulation and it will be described in paragraph 2.3.2.

The first calibration constraint was obtained by upscaling the GeoTOP model top surface, corresponding to 1000 years BP (prior to anthropogenic influences), to a grid size of 1 x 1 km conformable to the grid-resolution of the SFM grid size.

In order to obtain the net-to-gross at wells (the second calibration constraint) the GeoTOP model (figure 2a) was indicator-coded into a channel-overbank depositional facies model (figure 2b). The facies differentiation was performed by assigning a value of 1 net-to-gross to channel belt cells and 0 to overbank cells. Subsequently, net-to-gross data at four synthetic well locations was extracted from the net-to-gross model (figure 3a and 3b).

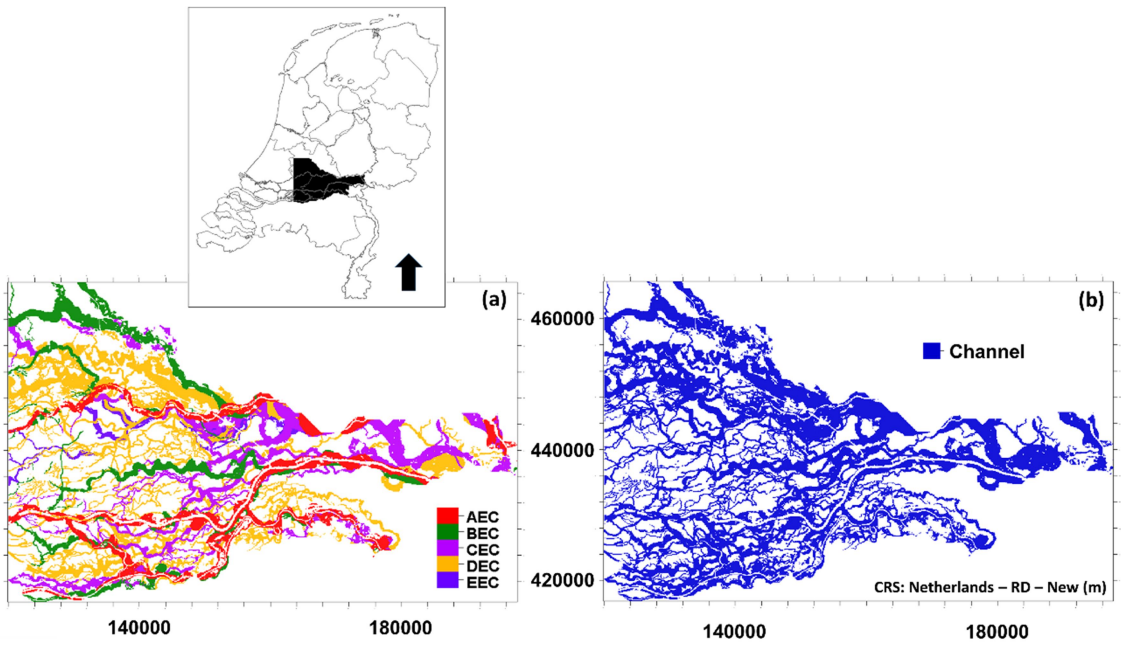

Figure 2: (a) Map view of the GeoTOP model with channel belt classification indicating relative ages (from younger to older: AEC, BEC, CEC, DEC, EEC); the (b) indicator-coded depositional model showing channel deposits only (Coordinate reference system: RD coordinates). In both models, the overbank fines have been made transparent.

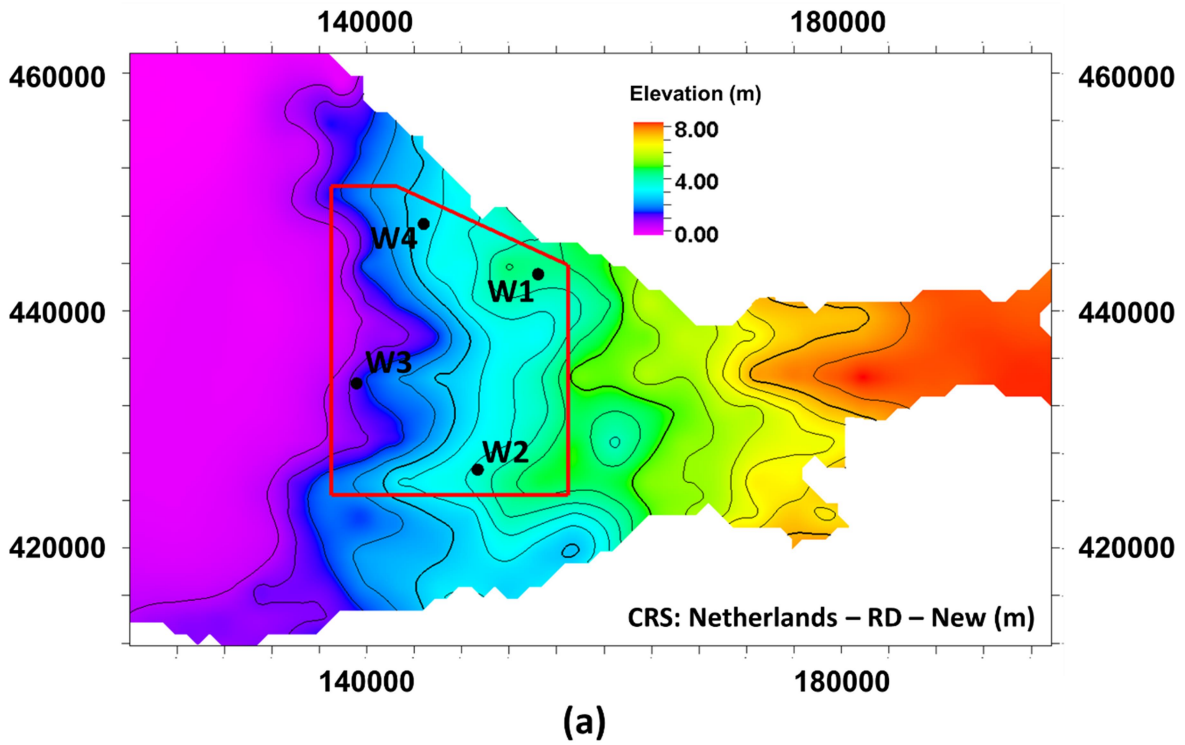

(a)

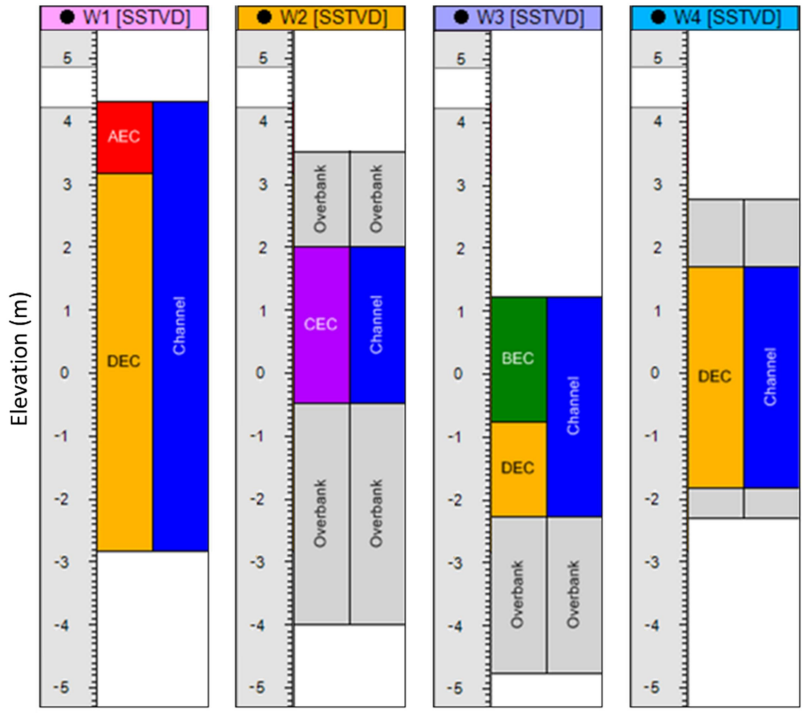

(b)

Figure 3: Calibration constraints. (a) Top surface (1000 years BP) of GeoTOP model with indication of the reservoir area and well locations (Coordinate reference system: Netherlands – RD – New); (b) depositional facies logs at the synthetic wells of the GeoTOP model (left column) and simplified indicator-coded depositional model which differentiates between channel and overbank facies (right column).

2.3 SFM description and setup

2.3.1 Model description

A basin-scale model of river-shelf evolution (Meijer, 2002) combined with a sub-grid parameterization of fluvio-deltaic processes and stratigraphy (SimClast: Dalman and Weltje, 2008, 2012) was used to simulate the stratigraphy. While the grid size (1 by 1 km in this study) used for basin simulations does not allow the model to resolve sedimentary structures on the scale of individual channel belts, the implicit (subgrid) sedimentary processes included do allow a more realistic sedimentary architecture to develop as compared to diffusive basin scale models. Sedimentary processes relevant for this study are included by sub-grid parameterization of avulsions and mouthbar-induced bifurcations. Avulsions occur as a consequence of channel belt aggradation and superelevation whereas mouthbar-induced bifurcations dominate the terminal parts of the sediment dispersal system where delta lobes grow and topographic gradients are low or the system enters the marine domain. In order to adequately test the new optimization routine (see paragraph 2.4) and keep the parameter space within feasible dimensions the numerical experiments in this study did not include sedimentary processes associated with coastal and backwater dynamics (e.g. waves and tides). This model version adequately represents sedimentary processes shaping the stratigraphy, as the area of interest is influenced only by fluvial and alluvial processes in the Rhine-Meuse deposits during the Holocene.

2.3.2 Setup

The well studied Rhine-Meuse deposits allows a multitude of controlling parameters to be used. Incorporating all would result in a high dimensional parameter space, thereby resulting in an order of magnitude increase of number of computational runs. Therefore simplifications were made by assuming space differential subsidence, temporal variations in sediment supply and water discharge out of scope for this study.

From the available dataset, several input parameters were extracted to be used in SimClast. Simulation time was set to 8000 years (9000 to 1000 years BP) corresponding to the main

accumulation phase of sediment in the Holocene Rhine-Meuse delta (Erkens et al., 2006; Hijma et al., 2009; Hijma et al., 2011). The initial topography, representing the top of the Rhine-Meuse fluvial paleovalley systems and its flanks at the onset of Holocene relative sea-level at ~9000 years BP, was taken from Koster et al. (2016) (figure 4). The surface represents an up-scaled version of a high-resolution (100 by 100 m) grid that is used internally in the GeoTOP model workflow. The surface extends over an area of 78 by 178 km and has a topographic elevation ranging from 13 to -27 m with an average slope of about 0.01° dipping to the west. The grid discretization used is 1×1 km as this scale is a good balance between data resolution and computer runtime. Two river inlet locations were used, for the Rhine and Meuse river systems, and values of sediment supply (*sl*) and water discharge (*q*) rate were assigned accordingly. The SimClast setup also required stream and diffusive transport set coefficients, representing sediment transport efficiency. Both the environmental parameters (*sl* and *q*) and the coefficients were investigated with preliminary sensitivity analyses meant to investigate the impact of each single unknown separately. To this end, a preliminary uncertainty range was assigned to the environmental parameters and the coefficients. The fixed ratio assumed between Meuse and Rhine environmental parameters was also object of sensitivity.

Starting from a base case, obtained by choosing for each unknown the mid value of its uncertainty range, SFM simulations were performed by varying only one unknown at a time, covering the uncertainty range with a loose sampling interval. The relative influence of each unknown was analyzed in terms of top surface elevation, average net-to-gross as well as channel layout. These sensitivity analyses showed that the sediment load, discharge, exponent of slope and stream coefficient had the most impact on the simulation results. These four parameters were assigned a range to explore the associated uncertainty while the other parameters were assigned a fixed value. In addition, from the results of the sensitivity analysis a ratio of 1/3 between Meuse and Rhine was individuated. Table 1 shows the fixed values assumed and the ranges explored for the main parameters of basin simulations used in the sensitivity analysis and in the subsequent stages. A mismatch exists between the sediment load and discharge values from literature (section 2.1) and the individuated used in SimClast. Therefore, the matching of SFM to real world results may show a strong non-uniqueness for the various outcomes. Nonetheless, the main objective of our work focused

on the matching routine, therefore further study should be addressed in improving the SimClast matching of the environmental parameters.

The river entry points were positioned along the eastern boundary of the initial surface and they were assumed to be fixed in time, a feature that is reasonable based on geological observations (Stouthamer et al., 2011). The sediment-supply consists of two discrete classes: sand and clay. Both the sediment entry locations and the sediment and water rates were time invariant for each simulation. The variation of the sea level was defined through the relative sea-level curve from Hijma and Cohen (2010) which describes the groundwater change over the considered simulation time.

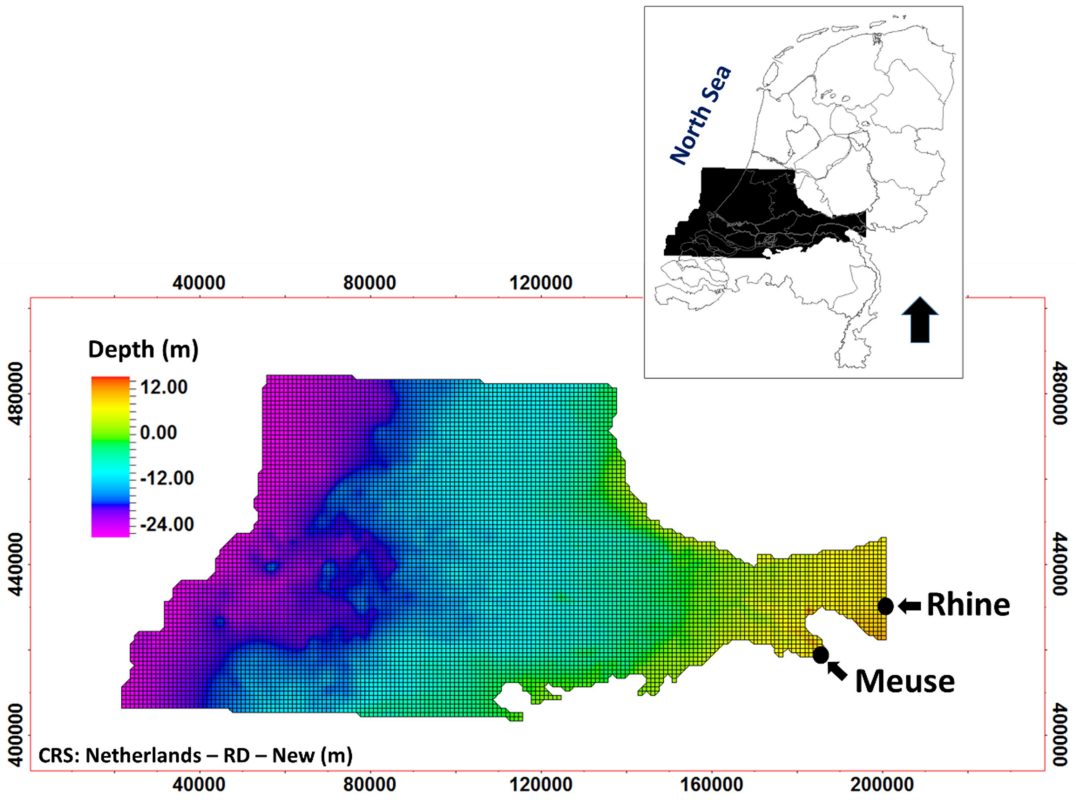

Figure 4: Model base surface (9000 years BP; Koster et al., 2016) used for basin simulations. The river inflow locations are indicated on the eastern boundary of the surface.

Table 1: Values and ranges of the main input parameters used for basin simulation.

Rhine sediment load (*kg/s*)	*sl*	70-120
Rhine discharge (m^3/s)	*q*	100 - 1500
Exponent of slope [-]	e_s	1 - 5
Stream coefficient [-]	c_s	0.1 - 8
Exponent of discharge [-]	e_d	1
Transport length deposition/erosion [-]	tl	1500
Threshold discharge [m/yr]	t_d	12.5

2.4 Matching routine

2.4.1 Neighborhood Algorithm

A variation of the direct-search gradient-free Neighborhood Algorithm (NA) (Sambridge 1999, 2001, Imhof and Sharma, 2006, 2007) was used to calibrate the SFM. This iterative sampling algorithm is applicable to a wide range of inversion problems, particularly those where the relationship between the observations and the unknowns (a finite number of model parameters) is complex and non-linear (e.g. Imhof and Sharma, 2006; Sambridge, 2001).

At the initial stage, the implemented algorithm generates n_S sets of uncertain model parameters by randomly sampling each parameter inside a user-specified range following a uniform distribution (table 1) and the corresponding stratigraphic models are simulated. The magnitude of the initial population (n_S) is generally set based on the number of searching dimensions (i.e. number of uncertain parameters, n). We set $n_S = n^{3.5}$, according to the empirical saturation value from Sambridge (2001), i.e. the minimum value of samples allowing the NA to perform well. Successively, for each sampled model output, the associated fitness is evaluated, based on the calibration constraints described in section 2.4.2. In optimization terminology, the initial set of sampled models is called initial population; the parameter space is a multidimensional domain delimited by the range of values for each uncertain parameter, where each parameter represents a searching dimension.

297 At each iteration, the entire parameter space is partitioned into a set of n-dimensional Voronoi cells,
298 where n is the number of uncertain parameters characterizing the model. Each cell delimits the nearest
299 neighbor region of an element of the current population, which is the cell centroid. Voronoi cells are
300 ranked according to the corresponding fitness, which is assumed to be constant within the cell and
301 equal to the fitness of the cell centroid (Sambridge 1999a). New parameter sets are sampled from both
302 low fitness cells and random ones; this allows the algorithm to shift the search to new areas of the
303 parameter space once low-error-model regions have been oversampled (i.e. local minima). This is a
304 strong point of the technique because it allows non-unique outcomes. For each of the selected
305 Voronoi cells new samples are generated by uniform random walk within the cell (Sambridge, 1999a,
306 1999b).
307 The new samples generated at each iteration are added to the population; the corresponding
308 stratigraphic models and fitness functions are calculated. As more models are added and evaluated,
309 the NA focusses on low-error areas of parameter space and densely sample these. The inversion
310 algorithm is run for several iterations until a stop criterion (a maximum number of iterations reached
311 or stagnation in the fitness function) is met.
312 The outcome of the inversion is an ensemble of diversified calibrated models rather than the lowest
313 error model.
314 The methodology is not well suited for high number of uncertain parameters because the
315 neighborhood search via the Voronoi approach loses efficiency; in fact, a high dimensionality results
316 in the data space being sparsely populated with data points. However, the NA has several advantages:

317 - it is a good compromise between exploration and exploitation
318 - it can manage multimodal functions (i.e. escape from local minima)
319 - it can obtain a plurality of calibrated models instead of a single best fit
320 - it considers all the previously attempted parameter combinations to produce new candidate
321 solutions
322 - it allows for straightforward parallelization

323
324

2.4.2 *Fitness function*

The outcome of SimClast simulations conducted for each sampled set of uncertain parameters is compared with the GeoTOP constraints. Two calibration constraints are considered (section 2.2): (1) the 1000 years BP top surface analogous to a seismic 2D surface information covering the area influenced only by fluvial and alluvial processes in the Rhine-Meuse delta; (2) the net-to-gross data at four synthetic wells, extracted from the GeoTOP model, located within a hypothetical reservoir area.

The cumulative goodness of fit is quantified by the total misfit with respect to these constraints, expressed by:

$$Error = \frac{RMSE_{surface} + RMSE_{wells}}{2} \quad (1)$$

where $RMSE_{surface}$ is the root mean square error between the elevation of GeoTOP top surface ($Z_{GeoTOPi}$) and the corresponding surface obtained by the stratigraphic forward model described in paragraph 2.3 (Z_{SFMi}); the quote difference was normalized with respect to the maximum reservoir thickness (max_H = 8 m):

$$RMSE_{surface} = \frac{\sqrt{\sum_{i=1}^{n_{points}} \left(\frac{Z_{GeoTOPi} - Z_{SFMi}}{max_H}\right)^2}}{n_{points}} \quad (2)$$

where n_{points} is the number of grid points discretizing the surface.

The normalizations applied make the contribution of such calibration constraints comparable with the well calibration and allowed to summarize them into a single fitness function.

Eq. 2 slightly differs from the fitness function based on top surfaces presented in Sacchi et al. 2014; no tolerance was considered here due to the relatively thin layer of sediment in the case study.

The root mean square error relative to well calibration reads:

$$RMSE_{wells} = \frac{\sqrt{\sum_{i=1}^{n_{wells}} (N_{GeoTOP\,i} - N_{SFM\,i})^2}}{n_{wells}} \quad (3)$$

where N is a binary parameter arising from the comparison of the average net-to-gross value at calibration wells ($\overline{NTG}$) with a threshold value (α=0.3):

$$N = \begin{cases} 1 \; if \; \overline{NTG} \geq \alpha \\ 0 \; if \; \overline{NTG} < \alpha \end{cases} \quad (4)$$

$N_{GeoTOP\,i}$ is calculated by averaging the arithmetic mean of the net-to-gross values at each calibration well (i) in the GeoTOP dataset ($\overline{NTG_{GeoTOP_i}}$), while $N_{SFM\,i}$ is calculated by averaging the net-to-gross value at each calibration well (i) in the modeled stratigraphy ($\overline{NTG_{SFM\,i}}$).

The above fitness functions (eq. 3) differ from the well calibration fitness functions proposed by Sacchi et al., 2015, which were based on well tops and lithological logs. To manage the scale difference between representativeness of the well (meter scale) and SFM (kilometer grid scale) information the comparison at the wells is made here in terms of N (eq.4) instead of lithological log or net-to-gross. In fact, Falivene et al (2014) observed that the representativeness problem could be mitigated by averaging over relatively large intervals. However, in the presented case the reservoir thickness is quite thin (8m in the thickest part) and the averaging was not sufficient to account for the uncertainty associated with well calibration data and the simplifications inherent to the SFMs, thus a threshold was introduced on the averaged values.

Figure 5 shows the application of the threshold to the net-to-gross map of the GeoTOP model in which only the cells containing net-to-gross above the threshold are considered channels.

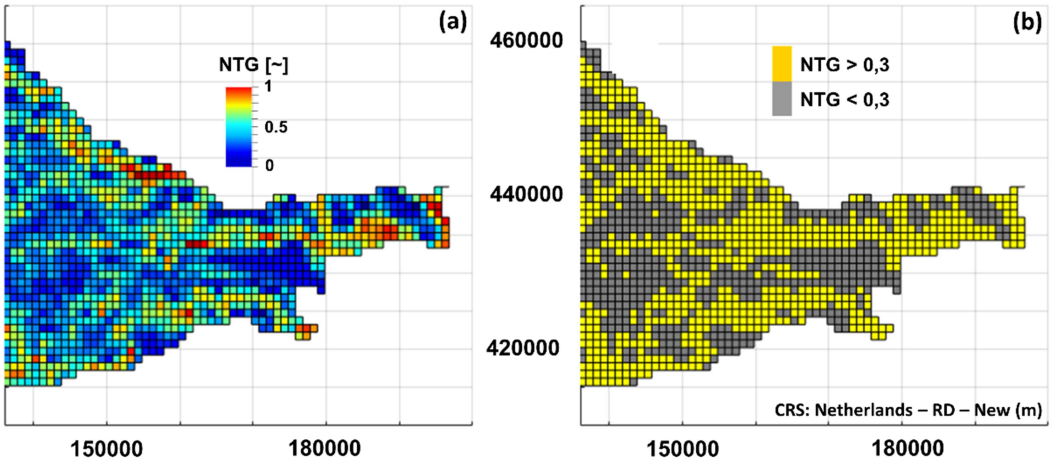

Figure 5: (a) Net-to-gross map derived from GeoTOP by upscaling the 100 m cells in Figure 2b to the 1 km cells of the model; (b) corresponding map with the threshold applied (Coordinate reference system: Netherlands – RD – New).

2.4.3 Two-stage optimization approach

The optimization process was performed over two hierarchical steps through the implementation of the NA. Preliminary sensitivity analyses (see section 2.3.2) were performed in order to identify the model parameters with the greatest influence on the outcome. Sediment load (*sl*) and discharge (*q*) turned out to dominate the SFM response in terms of fitness function value and visual inspection of the channel layout. Two other parameters showed a minor but significant impact on sediment transport efficiency in SimClast: the exponent of slope (e_s) and the stream transport coefficient (c_s) . This suggested the adoption of a 2-stage optimization approach: the problem is decomposed by first optimizing over a subset of the uncertain parameters that most significantly influence the model realization and then optimizing over the remaining significant uncertain parameters, thus reducing complexity:

- Step 1: optimization with respect to the uncertain parameters with highest impact on level of fitness (*sl* and *q*)
- Step 2: optimization with respect to the remaining uncertain parameters (e_s and c_s), in this step *sl* and *q* values from the previous step are assumed constant

This approach allows us to mitigate the main disadvantage of NA, i.e. the loss of performance related to the gradually increasing size of parameters space.

The comparison between the 1-stage and 2-stage approaches is illustrated in figure 6.

In order to locate multiple acceptable regions in parameter space and thereby addressing the inherent non-uniqueness in geological synthetic models; Step 2 was run for a number of different promising *sl* and *q* combinations identified in Step 1. In order to identify clusters of potentially valid parameters combinations from the final population of Step 1, along with the best sampled solution, two other

401 samples were selected based on a trade-off between the corresponding error and the parameter
402 diversity from the best solution. This selection process was manually done by visual inspection of the
403 Voronoi diagram of the fitness map (fig. 7); automation of the selection of promising parameters sets
404 will be part of future developments.
405 The proposed 2-stage NA approach with 4 parameters optimized sequentially in groups of 2 (i.e. 2
406 parameters optimized at each step) was compared with the 1-stage NA approach, with four parameters
407 optimized simultaneously. In both cases, the explorative feature of the algorithm was emphasized by
408 spreading the samples over several NA cells: at each iteration, new models in number equal to half of
409 the initial population were generated, each extracted from a different Voronoi cell. In order to avoid
410 trapping in local minima, 1/4 of the resampled cells were chosen from the fitness ranking, while 3/4
411 were chosen randomly from the remaining cells. The above relationships were calibrated against
412 analytical multidimensional multimodal test functions: Styblinski–Tang function (Styblinski and
413 Tang, 1990), Rosenbrock function (Rosenbrock, 1960), Holder table (Mishra, 2006), Bukin function
414 n°6 (Bukin, 1997) in a preliminary validation phase.
415
416
417

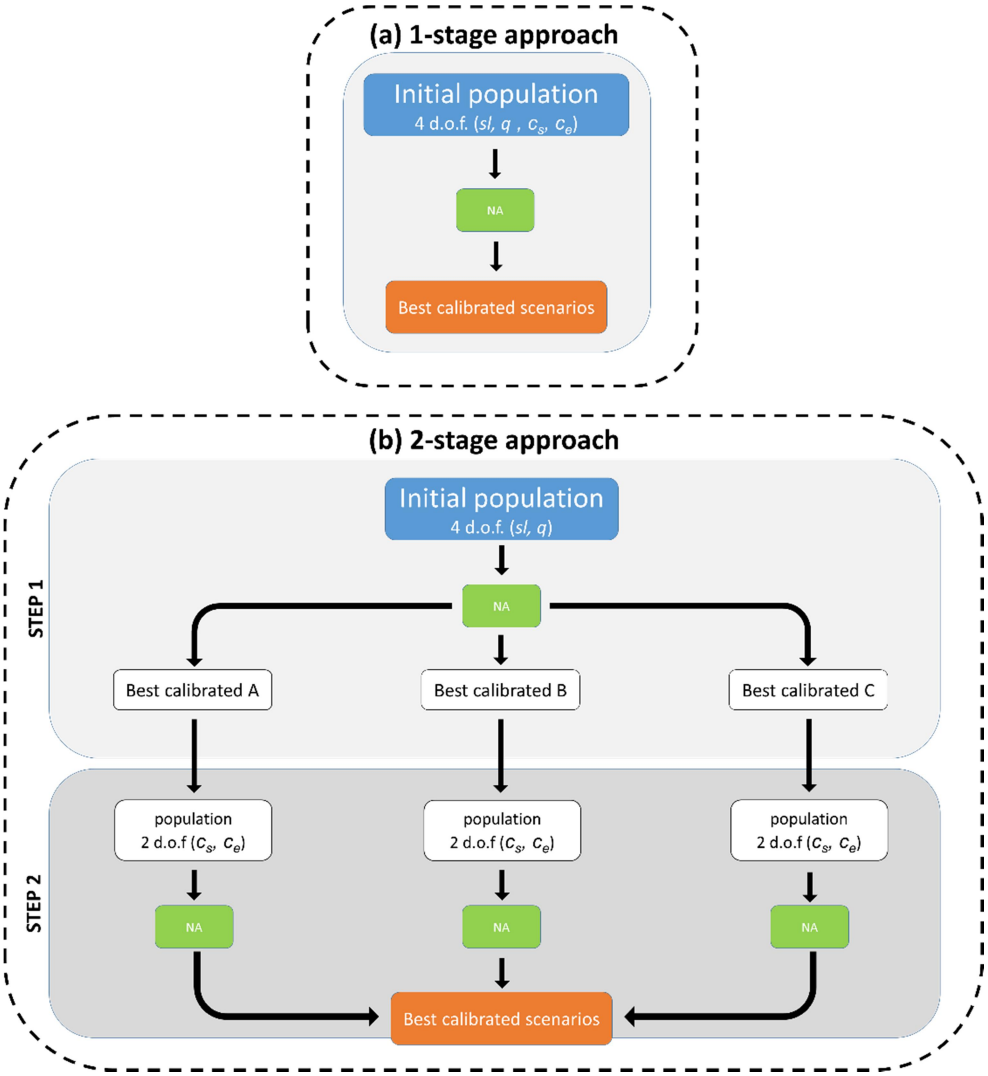

Figure 6: Comparison between the flowchart of (a) 1-stage with 4 degrees of freedom (d.o.f.) and (b) 2-stage optimization approach with 2 degrees of freedom. The dashed boxes refer to the inversion process box in figure 1.

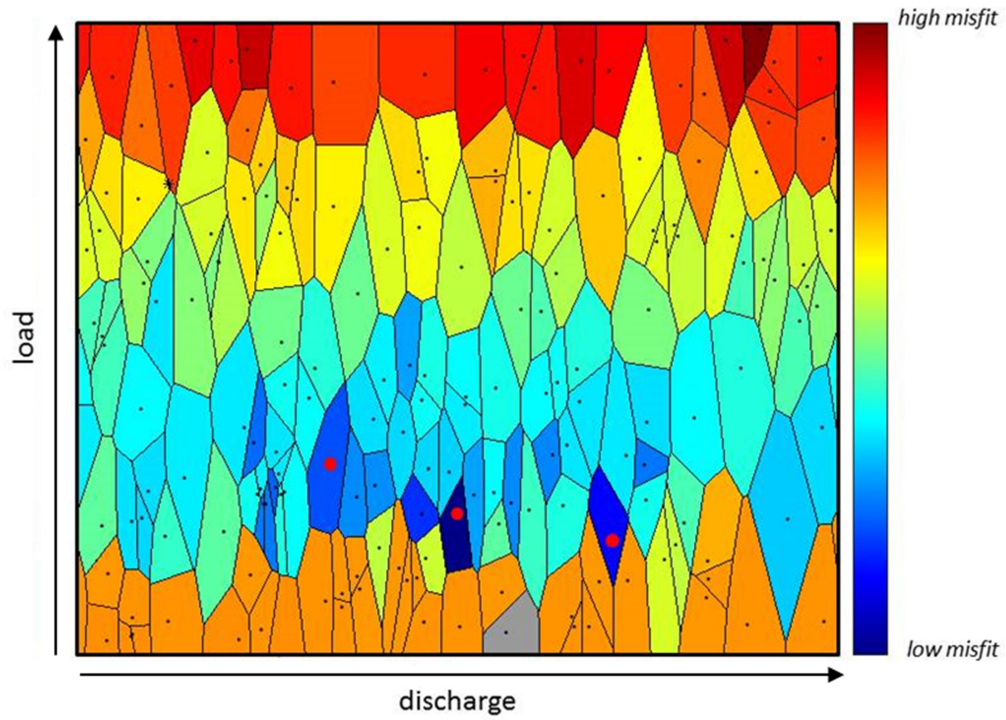

425

426

427

428 Figure 7: Example of qualitative Voronoi map with identification of local minima (red dots). A fixed
429 ratio between the Meuse and Rhine values is assumed. The forward model appears to be more
430 sensitive to the sediment load but the water discharge has a significant impact as well.

431

432

433

434 **3. Results**

435 The first part of the work concentrated on the comparative analysis of the proposed 2-stage NA
436 approach with respect to the 1-stage NA approach, (paragraph 2.4.3) evaluating their capability to
437 sample a range of valid models that are consistent with typical calibration constraints. The
438 optimization results were compared in terms of evolution of the fitness function with the number of
439 models sampled during the iterative process. The error evolution is obtained by selecting the error at
440 each iteration corresponding to the element of the current population exhibiting the best fitness, and

plotting it against the population cardinality (i.e. number of sampled models). Figure 8 illustrates an example of the evolution of fitness function (gray line) compared with the evolution of each calibration constraint (well calibration, green line, and top surface calibration, orange line) for the first step of 2-stage NA approach. The fitness function (grey line) consistently decreases as the population grows with iterations, while the evolution of each calibration constraint is not necessarily consistently decreasing (e.g. orange line) because one of the two calibration constraints can decrease in fitness if it is compensated by a significant improvement of the other calibration constraint.

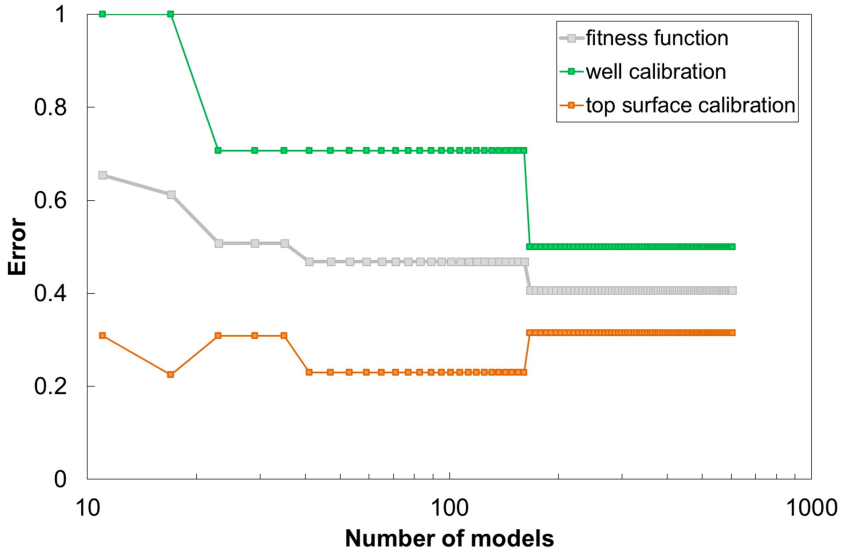

Figure 8: Evolution of the fitness function (gray line) compared with the evolution of each calibration constraint (well calibration, green line, and top surface calibration, orange line) for the first step of the 2-stage NA approach; squares represent the iterations.

Figure 9 shows the comparison between the error convergence curves produced by the two optimization approaches. The 1-stage approach is represented by a unique blue dotted line. The 2-stage approach, instead, shows a branch from the first step, characterized by a single red line, to the second step, characterized by three different lines (yellow, orange and brown) associated with the three sets of fixed environmental parameters (sediment load and discharge), named Case A, Case B and Case C respectively, selected among the final population of Step 1 based on the trade-off between error value and parameter diversity from the best solutions (section 2.4.3). Notice that Case A shows continuity of the error convergence curve between Step 1 and Step 2 because this scenario starts from the set of parameters that exhibits the lowest error among the population of Step 1. Conversely, for

Case B and Case C a discontinuity is observed on the error convergence curve between Step 1 and Step 2 because these scenarios start from two different sets of parameters explored in Step 1, which are promising (i.e. higher error than the best solution of step1) but characterized by a higher error with respect to the best solution of Step 1.

As described in paragraph 2.4.3, the initial number of the sampled models (i.e. initial population) is calculated as a function of the parameters that are used in the inversion algorithm (i.e. number of searching dimensions) and this explains why this number is much higher in the 1-stage (100) compared to the 2-stage approach (11). The cardinality of the initial population, in turn, affects the initial error value, which corresponds to the fitness of the best sample among the initial population. As more models are added and evaluated through the iterations, all the curves converge towards low error areas of the parameter space.

Table 2 shows the set of environmental parameters and coefficients used to simulate both the 1-stage and the 2-stage scenarios.

Table 3 shows the average net-to-gross values at each well location for the 1-stage and 2-stage approaches while table 4 shows the average top surface misfit for the 1-stage and 2-stage approaches. The top surface misfit is obtained by calculating the differences in altitude at each grid surface map location along the vertical direction. The results show that the 2-stage Case C scenario has the lowest average net-to-gross misfit with respect the reference GeoTOP while the average surface misfit is comparable in all the cases. The matching of the wells seems to have a random behavior, in fact we did not observe a systematic problem in matching specific wells. As a way of example the top surface misfit maps for the 1-stage and 2-stage scenarios are shown in figure 10.

Figure 11 shows net-to-gross maps of the reference case as well as of the simulated scenarios for both the 1 and 2-stage approaches (Case A-B-C). All simulated maps show realistic representation of convergent and divergent fluvial channel patterns typical of a distributary network.

Table 2: Set of optimal environmental parameters and coefficients obtained from the 1-stage and the 2-stage scenarios.

	1-stage	2-stage (Step 1)	2-stage (A)	2-stage (B)	2-stage (C)
Rhine sediment load (*kg/s*)	58	54	54	49	66
Rhine discharge (m^3/s)	1110	689	689	774	327
Exponent of slope [-]	3.85	2.38	1.95	2.64	3.92
Stream coefficient [-]	5.84	5.78	1.54	2.66	7.51

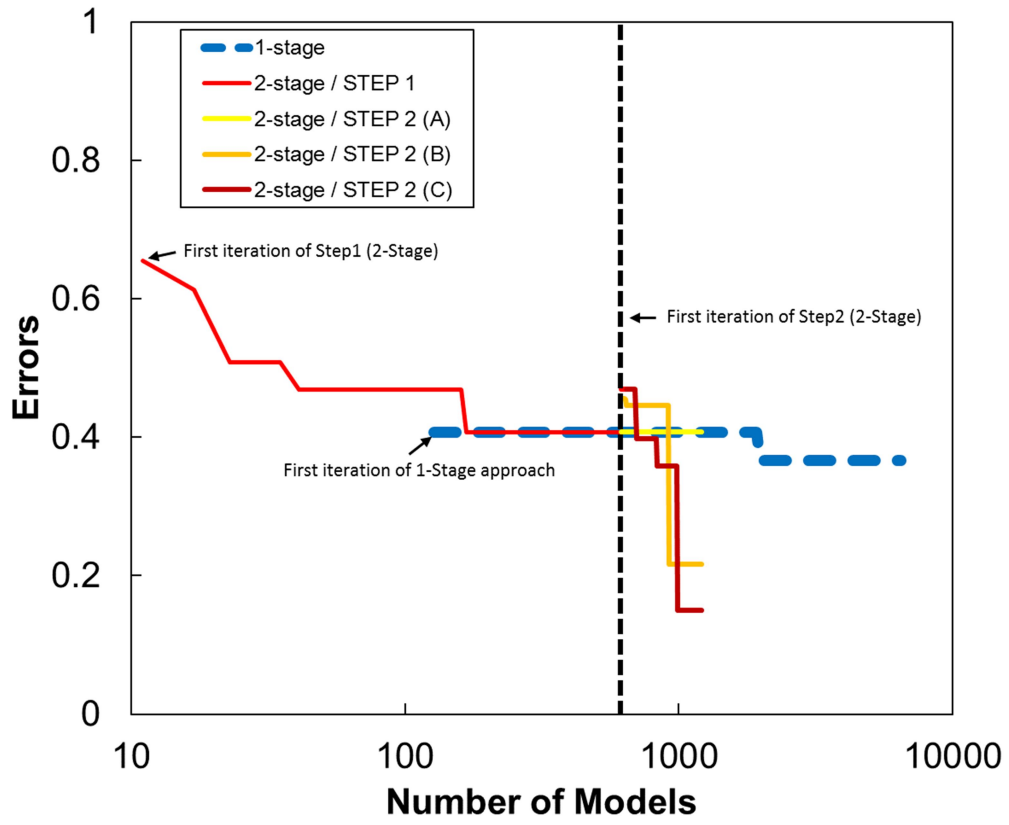

Figure 9: Comparison between the error convergence curves produced by the 1-stage approach (blue) and the 2-stage approach which is composed by a first step (red) and a second step, characterized by three different lines (yellow, orange and brown) associated to the 3D set of fixed environmental parameters (sediment load and discharge).

Table 3: Average net-to-gross at wells for the 1-stage and 2-stage approaches

	Well 1	Well 2	Well 3	Well4
GeoTOP	0.5	0.42	0.51	0.5
1-stage	0.38	0.36	0.39	0.41

2-stage_Case a	0.48	0.38	0.39	0.4
2-stage_Case b	0.38	0.39	0.37	0.43
2-stage_Case c	0.48	0.44	0.43	0.46

501

502 Table 4: Average top surface misfit for the 1-stage and 2-stage approaches with respect to GeoTOP

	Average Misfit (m)
1-Stage	2.96
2-stage_Case a	3.02
2-stage_Case b	3.6
2-stage_Case c	3.2

503

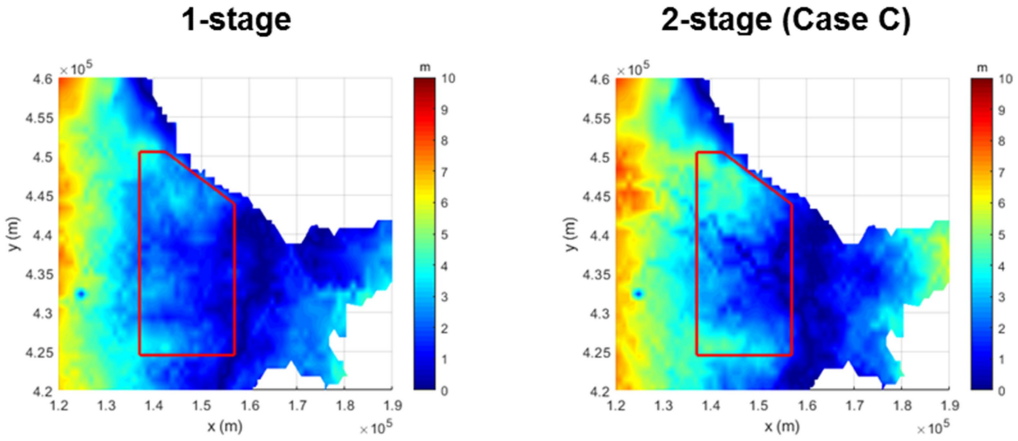

504

505 Figure 10: Surface misfit for the 1-stage (left) and the 2-stage Case C scenarios. The misfit map is

506 obtained by vertically subtracting the altitude at each grid location. The red polygon indicates the

507 hypothetical reservoir area.

508

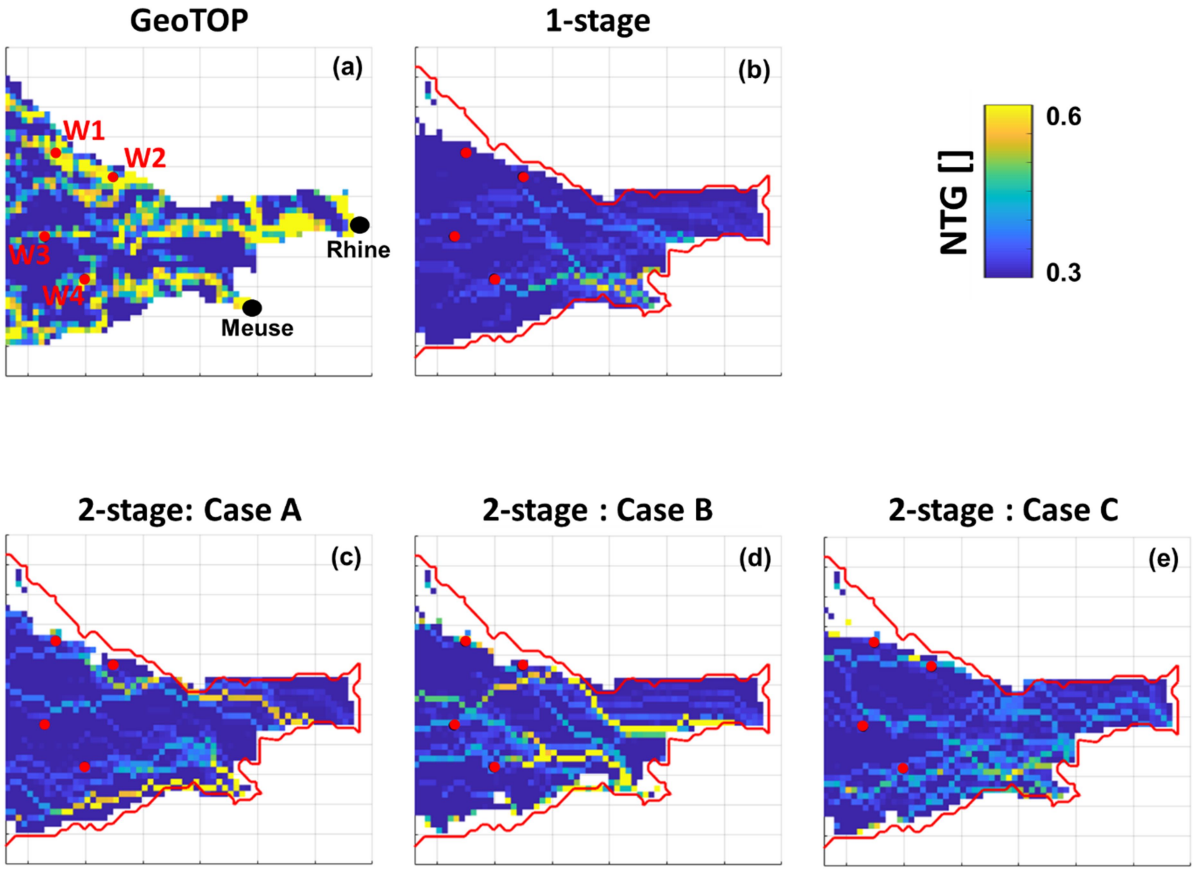

Figure 11: (a) Upscaled GeoTOP net-to-gross map (1 km grid); (b) simulated net-to-gross map using the 1-stage approach; (c) (d) (e) three best net-to-gross map scenario obtained using the 2-stage approach (from left to right Case A, Case B and Case C). The color scale ranges between 0.3 and 0.6 net-to-gross in order to highlight the channel belts geometries. The well locations are indicated with red dots while the contour line of the GeoTOP top surface is indicated with the red line.

3.1 Stratigraphic expression of calibrated simulations

The SFM records very high resolution vertical stratigraphic intervals (averaged over grid cells of ~1 mm thickness). In order to compare with the GeoTOP data this stratigraphy is upscaled. Figure 12 shows both the actual synthetic stratigraphy with net-to-gross property of one example gridcell after a typical simulation and the upscaled net-to-gross. Although upscaled net-to-gross property is used to compare with the GeoTOP model at well locations, actual high resolution net-to-gross stratigraphic

523 expression output by the SFM may still be used for other purposes such as detailed constraining of
524 reservoir models.

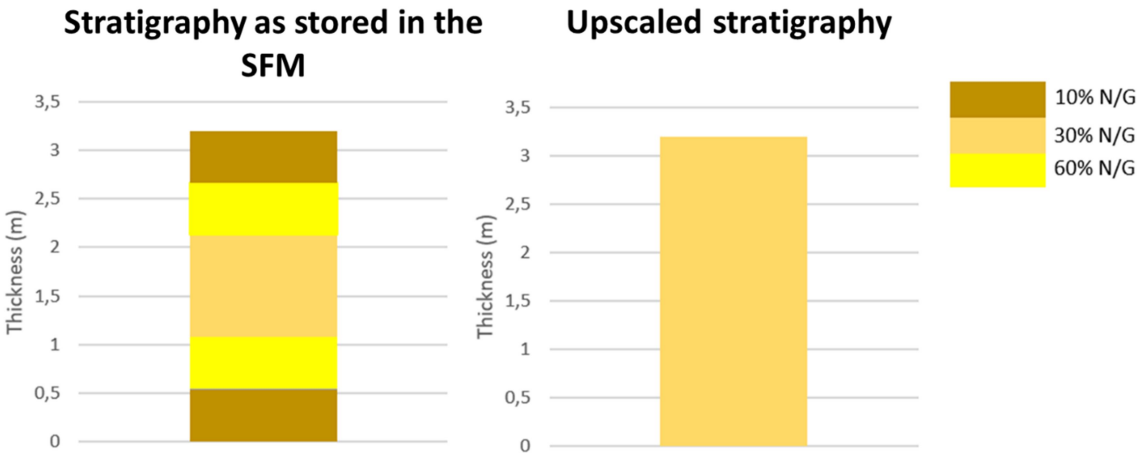

525
526
527 Figure 12: Example of synthetic stratigraphy in one gridcell generated by the SFM (left) showing the
528 low net-to-gross units at base and top, sandy units in yellow and mixed units in orange. Upscaled
529 stratigraphy as extracted from the high resolution stratigraphy (right).
530
531 The stratigraphic output of the SFM is highly variable. The misfit of the 1-stage example run and the
532 best 2-stage run (Case C) is shown in map view in figure 10. This shows that there is a significant
533 variability in realizations after calibration of further parameter sets.
534
535
536
537 **4. Discussion and conclusions**
538 ***4.1 Matching optimization***
539 The results outlined above show the possibility of matching lithological variations simulated with a
540 basin-scale SFM to real data. In this numerical framework, accurate estimation of the SFM input
541 parameters, especially initial topography and sediment entry points, ensured a reliable prediction of
542 the spatial distribution of channelized deposits (Sacchi et al., 2015).

543 The results demonstrate that a significant improvement is obtained by implementing the novel two-
544 step optimization approach as compared to the approach using four variables simultaneously. In fact,
545 with the same number of sampled models the error is significantly lower (Case B and C) or nearly
546 equal (Case A) to the one produced by the 1-stage approach; moreover the 1-stage approach did not
547 succeed in obtaining results comparable with Case B or C even with a significantly larger number of
548 samples. This demonstrates that a hierarchical exploration of the variable space can be very efficient.
549 A small variation in one of the two leading parameters can have a greater impact on the fitness
550 function value than a variation of one of the two other parameters, thus masking possible progress due
551 to explorations in the remaining directions. On the other side the search space of each optimization
552 step of the 2-stage approach is much reduced with respect to the 1-stage, thus allowing better
553 exploration. The choice of using multiple starting points for the second step of the 2-stage approach
554 proved to be valuable to escape from the local minimum at the end of Step 1. In fact, Case A, which
555 uses the optimum arising from Step 1 to fix values of sediment load and discharge is trapped in the
556 local minimum while Case B and C are able to further improve the sampling.
557
558 ***4.2 The stratigraphic variability in model output***
559 The outcome of the inversion process is an ensemble of diversified calibrated models, which
560 inherently capture a range of uncertainty. The uncertainty range largely depends on the amount and
561 type of data available as calibration constraints (i.e. well logs, well tops, seismic data). As illustrated
562 in figure 10 the difference in output of the model runs shows the strong non-uniqueness of the fluvial
563 sedimentary architecture despite only varying two parameters. This gives rise to the idea that the
564 diversified calibrated models may be combined to construct a set of probability density cubes of likely
565 net-to-gross occurrence to be used as a soft conditioning, as proposed by Sacchi et al. (2016), for
566 constraining reservoir scale models. Moreover, a Monte Carlo style post processing routine perturbing
567 the calibrated models outcome may be added to account for the natural variability inherent in the
568 sedimentary record which a deterministic SFM cannot capture. The interpretation of ancient deposits
569 is many faceted, this is shown by the mismatch between the best fit sediment loads and discharge
570 values in the model results (table 2) with the reference case (Figure 10). The outcome of our work in

matching SFM to real world results may show a strong non-uniqueness for the various outcomes. However, the focus of this study is on optimizing the matching routine. Further optimization to match the N/G maps (see Figure 10) and expanding on this subject is proposed for further study.

4.3 Geological constraints

Wave reworking enhances large-scale depositional connectivity by producing laterally extensive sandy plains and beach-ridge complexes (Reynolds, 1999; Hampson, 2000). Similarly, tidal currents tend to increase depositional connectivity by forming elongated sand bodies perpendicular to the shoreline. However, the net effect of tidal activity becomes difficult to predict because it regulates local accumulation of fine-grained sediments, which may affect the morphodynamic evolution of the entire delta (Edmonds and Slingerland, 2010). These coastal processes will have a direct influence on upstream fluvial processes in the modelled area by effectively changing the baselevel and sediment transport capacities of the channels in question.

The mixing of sand with clay, peat formation and post-depositional processes (i.e. differential subsidence) complicate further predictions of incision and sedimentation patterns in tidally influenced distributary channels. Despite these potential problems, groundwater regime in the studied part of the Holocene Rhine-Meuse was river-dominated (Koster et al., 2016). Thus, based on sedimentological evidence it is not unreasonable to assume that our modelling approximations represented the sedimentary evolution in the study area fairly well as the area in question was influenced to a lesser extent by major peat deposition or tidal influence but was purely fluvial at time of deposition. Peat deposition has been shown to stabilize the channel belts further, decreasing lateral migration and increase the rate of filling by peat growth.

4.4 Future work

The workflow proposed in this study may be applied to deep, data sparse, reservoir or aquifers in order to populate static geological models with sedimentary properties derived from the calibrated SFM output. An additional use of SFM matched to real world data sets is by allowing conceptual theories to be tested and quantified. i.e. the current model may be used to test models of avulsion

599 frequency in the Holocene Rhine Meuse fluvial system (Stouthamer et al 2011).
600 The challenge of predicting reservoir-quality distribution in channelized reservoirs requires detailed
601 knowledge about sediment-body geometry and heterogeneity at different scales (Martinius et al.,
602 2014). From this viewpoint, large-scale depositional connectivity which may be captured using the
603 basin-scale SFM needs to be complemented by quantifiable information about the 3D geometry of
604 architectural elements (i.e. channels, point bars, levees and crevasse splays) and their degree of
605 amalgamation (sensu Peter et al., 2017). In addition, the spatial distribution of geological properties
606 (e.g. petrophysical) need to be well described in order to more accurately predict reservoir-quality
607 distribution. In that respect, future developments should focus on integrating post-depositional
608 processes in SFMs, and in particular differential subsidence, tectonic control and early diagenetic
609 alterations by means of reactive transport modelling. Further study should also focus on the automatic
610 identification of the number of potential local minima that can be retained in the first stage of the
611 optimization procedure (Step 1). A possible approach could be to use a density-based clustering
612 algorithm, such as DBSCAN or OPTICS (Ester et. al, 1996; Ankerst et al., 1999) on a subsample of
613 the sampled population obtained by applying cut-off values to the objective functions based on the top
614 surface calibration (eq. 2) and well calibration (eq. 3) or to the combined error function (eq. 1).
615
616
617 **Computer code availability**
618 The related code is written in MATLAB 2018. The file name of related code is "NA_Basin". To
619 access the source file of the code, one can visit the repository on GitHub (https://github.com/REDD-
620 PoliTO/Optimization).
621
622 **Acknowledgments**
623 We express our gratitude to Prof. Gert Jan Weltje from KU Leuven for his support during the initial
624 conceptualization and development stages of the project .
625

626 **References**

627 Ankerst, M., Breunig, M. M., Kriegel, H. P., & Sander, J. (1999). OPTICS: ordering points to identify
628 the clustering structure. ACM Sigmod record, 28(2), 49-60.
629
630 Berendsen, H.J.A. and E. Stouthamer 2001, Palaeogeographic development of the Rhine-Meuse delta,
631 the Netherland, Assen (Van Gorcum)
632
633 Bertonello, A., Sun, T., Li, H., Mariethoz, G. and Caers, J. (2013) Conditioning Surface-Based
634 geological Models to Well and Thickness data. Mathematical geosciences, 45(7), 873-893. DOI:
635 10.1007/s11004-013-9455-4
636
637 Bukin, A.D. (1997). New Minimization Strategy For Non-Smooth Functions, Budker Institute of
638 Nuclear Physics preprint BUDKER-INP-1997-79, Novosibirsk.
639
640 Charvin, K., Gallagher, K.L., Hampson, G. and Labourdette, R. (2009). A Bayesian approach to
641 inverse modelling of stratigraphy, part I: method. Basin Research, 21, 5–25.
642
643 Cohen, K.M., Stouthamer, E., 2012. Digitaal Basisbestand Paleogeografie van de Rijn-Maas Delta.
644 DANS. https://doi.org/10.17026/dans-x7g-sjtw.
645
646 Cross, T. and Lessenger, M. (1999). Construction and application of stratigraphic inverse model. In:
647 Harbaugh, J.W. et al. (eds.), Numerical Experiments in Stratigraphy: Recent Advances in
648 Stratigraphic and Sedimentologic Computer Simulations. SEPM Special Publication 62, 69-83.
649
650 Dalman, R.A.F. and Weltje, G.J. (2008). Sub-grid parameterisation of fluvio-deltaic processes and
651 architecture in a basin-scale stratigraphic model. Computers & Geosciences, 34, 1370–1380.
652
653 Dalman, R.A.F. and Weltje, G.J. (2012). SimClast: An aggregated forward stratigraphic model of
654 continental shelves. Computers & Geosciences, 38, 115-126.
655
656 Deutsch, C.V. (2002). Geostatistical Reservoir Modeling. Oxford University Press, Oxford, 376 p.
657
658 Edmonds, D.A. and Slingerland, R.L. (2010). Significant effect of sediment cohesion on delta
659 morphology. Nat. Geosci. 3, 105–109.
660

661 Erkens, G., Cohen, K.M., Gouw, M.J.P., Middelkoop, H. and Hoek, W.Z. (2006). Holocene sediment
662 budgets of the Rhine Delta (The Netherlands): a record of changing sediment delivery. IAHS
663 Publication, 306, 406-415.
664
665 Ester, M., Kriegel, H. P., Sander, J., and Xu, X. (1996). A density-based algorithm for discovering
666 clusters in large spatial databases with noise. In Kdd, 96(34), 226–231.
667
668 Falivene O., Frascati A., Gesbert S., Pickens J., Hsu Y., and Rovira A. (2014). Automatic calibration
669 of stratigraphic forward models for predicting reservoir presence in exploration. AAPG Bulletin, V.
670 98, No. 9 (September 2014), 1811–1835. The American Association of Petroleum Geologists. doi:
671 10.1306/02271413028.
672
673 Granjeon, D. and Joseph, P. (1999). Concepts and applications of a 3-D multiple lithology, diffusive
674 model in stratigraphic modeling. In: Harbaugh, J.W. et al. (eds.), Numerical Experiments in
675 Stratigraphy: Recent Advances in Stratigraphic and Sedimentologic Computer Simulations, SEPM
676 Special Publication 62, 197– 210.
677
678 Hijma, M.P., Cohen, K.M., 2010. Timing and magnitude of the sea-level jump preluding the
679 8200 yr event. Geology 38 (3), 275-278.
680
681 Hijma, M.P. and Cohen, K.M. (2011). Holocene transgression of the Rhine river mouth area, the
682 Netherlands/Southern North Sea: palaeogeography and sequence stratigraphy. Sedimentology, 58,
683 1453–1485.
684
685 Hijma, M.P., Cohen, K.M., Hoffmann, G., Van der Spek, A.J.F. and Stouthamer, E. (2009). From
686 river valley to estuary: the evolution of the Rhine mouth in the early to middle Holocene (western
687 Netherlands, Rhine-Meuse delta). Neth. J. Geosci., 88(1), 13–53.
688
689 Karamitopoulos, P., Weltje, G.J. and Dalman, R.A.F. (2014). Allogenic controls on autogenic
690 variability in fluvio-deltaic systems: Inferences from analysis of synthetic stratigraphy. Basin
691 Research, 26(6), 767-779. DOI: 10.1111/bre.12065.
692
693 Karssenberg, D., Tornqvist, T. and Bridge, J.S. (2001). Conditioning a process-based model of
694 sedimentary architecture to well data. Journal of Sedimentary Research 71, 868-879.
695

Karssenberg, D., De Vries, M. and Bridge, J.S. (2007). Conditioning a process-based fluvial-stratigraphy model to well data by inverse estimation of model inputs using a genetic algorithm. AAPG Search and Discovery Article #90063, AAPG Annual Convention, Long Beach, California.

Koster, K., Stafleu, J. and Cohen, K.M. (2016). Generic 3D interpolation of Holocene base-level rise and provision of accommodation space, developed for the Netherlands coastal plain and infilled paleovalleys. Basin Research, 1-23. doi:10.1190/1.2720496.

Imhof, M.G. and Sharma A.K. (2007). Seismostratigraphic inversion: Appraisal, ambiguity and uncertainty: Geophysics, v. 72, R51–R66, doi:10.1111/bre.12202.

Imhof, M. and Sharma, A.K. (2006). Quantitative seismostratigraphic inversion of a prograding delta from seismic data: Marine and Petroleum Geology, 23, 735–744, doi:10.1016/j.marpetgeo.2006.04.004.

Hampson, G.J. (2000). Discontinuity, surfaces, clinoforms, and facies architecture in a wave-dominated, shoreface-shelf parasequence. Journal of Sedimentary Research, 70, 325-340.

Hajek, E.A. and Wolinsky, M.A. (2012). Simplified processmodeling of river avulsion and alluvial architecture: Connecting models and field data. Sedimentary Geology, 257-260, 1-30. https://doi.org/10.1016/j.sedgeo.2011.09.005.

Hijma, M.P. and Cohen, K.M. (2006). Timing and magnitude of the sea-level jump preluding the 8200 yr event. Geological Society of America, 38 (3), 275-278, doi:10.1030/G30439.1.

Maljers, D., Stafleu, J., Van der Meulen, M.J. & R.M. Dambrink (2015) Advances in Constructing Regional Geological Voxel Models, Illustrated by their Application in Aggregate Resource Assessments. Netherlands Journal of Geosciences. 94. p. 257-270.

Martinius, A.W., Howell, J.A., and Good, T. (2014). Sediment-Body Geometry and Heterogeneity: Analogue Studies for Modelling the Subsurface. Geological Society Special Publications 387, p. 299.

Meijer, X.D. (2002). Modelling the drainage evolution of a river-shelf system forced by Quaternary glacio-eustasy. Basin Research, 14, 361–377.

Mishra, S. (2006). Some new test functions for global optimization and performance of repulsive particle swarm method. ACM Transactions on Modeling and Computer Simulation.

Paola, C. (2000). Quantitative models of sedimentary basin filling. Sedimentology, 47, 121–178.

Peter, C., Sacchi, Q., Serazio, C. and Verga, F. (2017). Capturing channelized reservoir connectivity uncertainty with amalgamation curves. Marine and Petroleum Geology, 88, 329-342. https://doi.org/10.1016/j.marpetgeo.2017.07.017.

Reynolds, A.D. (1999). Dimensions of Paralic Sandstone Bodies. In: AAPG Bulletin, 83, 211-229.

Rosenbrock, H.H. (1960). An automatic method for finding the greatest or least value of a function. The Computer Journal. 3 (3): 175–184. doi:10.1093/comjnl/3.3.175. ISSN 0010-4620.

Sacchi, Q., Weltje, G.J. and Verga, F. (2015). Towards process-based modelling: Obtaining basin-scale constraints from seismic and well data. Marine and Petroleum Geology, 61, 56-68.

Sacchi, Q., Borello, E.S., Weltje, G.J. and Dalman, R.A.F. (2016). Increasing the predictive power of geostatistical reservoir models by integration of geological constraints from stratigraphic forward modelling. Marine and Petroleum Geology, 69, 112-126.

Sambridge, M. (1999). Geophysical inversion with a neighborhood algorithm–Searching a parameters space: Geophysical Journal International, 138, 479–494, doi:10.1046/j.1365-246X.1999.00876.x.

Sambridge, M. (2001). Finding acceptable models in nonlinear inverse problems using a neighborhood algorithm: Inverse Problems, 17, 387–403, doi:10.1088/0266-5611/17/3/302.

Sambridge, M., and K. Mosegaard (2002). Monte Carlo methods in geophysical inverse problems: Reviews of Geophysics, 40, 1–29. doi: 10.1029/2000RG000089.

Sharma, A. K. (2006). Quantitative stratigraphic inversion, Ph.D. Dissertation, Virginia Polytechnic Institute and State University, Blacksburg, Virginia, 91 p.

Stafleu, J., Maljers, D., Gunnink, J.L., Menkovic, A. and Busschers, F.S. (2011). 3D modelling of the shallow subsurface of Zeeland, the Netherlands. Netherlands Journal of Geosciences 90, 293–310.

Stafleu, J., Maljers, D., Busschers, F.S., Gunnink, J.L., Schokker, J., Dambrink, R.M., Hummelman, H.J. & M.L. Schijf (2012) *GeoTOP modellering (in Dutch).* TNO Report TNO-2012-R10991, 216 p.

Stafleu, J. & C.W. Dubelaar (2016) Product Specification Subsurface model GeoTOP. TNO Report 2016 R10133 v1.3, 53 p.

Stafleu, J. and F.S. Busschers, 2017. Analysing lithological and grain-size trends using a 3D voxel model: a case study from the Holocene Rhine-Meuse delta (Extended Abstract, 5 pp). 79th EAGE Conference & Exhibition 2017 – Workshop Programme, Paris, France, 12-15 June 2017.

Stouthamer, E., Cohen, K.M. and Gouw, M.J.P. (2011). Avulsion and its implications for fluvial-deltaic architecture: insights from the holocene rhine–meuse delta. In: From River To Rock Record: The Preservation Of Fluvial Sediments And Their Subsequent Interpretation. SEPM Special Publication No. 97, 215-231.

Styblinski, M. and Tang, T. (1990). Experiments in Nonconvex Optimization: Stochastic Approximation with Function Smoothing and Simulated Annealing, Neural Networks, 3, 467-483.

Van der Meulen, Michiel and Doornenbal, J.C. and Gunnink, Jan and Stafleu, Jan and Schokker, Jeroen and Vernes, R.W. and Geer, Frans and Gessel, S.F. and Heteren, Sytze and Leeuwen, R.J.W. and Bakker, Marcel A.J. and Bogaard, Paul and Busschers, F.s and Griffioen, J. and Gruijters, S.H.L.L. and Kiden, Patrick and Schroot, B.M. and Simmelink, HJ and Berkel, W.O. and Daalen, T.M.. (2013). 3D geology in a 2D country: Perspectives for geological surveying in the Netherlands. Netherlands Journal of Geosciences - Geologie en Mijnbouw. 92. 217-241. 10.1017/S0016774600000184.

Weltje, G.J., Dalman, R.A.F., Karamitopoulos, P., Sacchi, Q. (2013). Reducing the uncertainty of static reservoir models: implementation of basin-scale geological constraints. Spe-164821-ms.

Wijns, C., Poulet, T., Boschetti, F., Dyt, C., Griffiths, C.M. (2004). Interactive inverse methodology applied to stratigraphic forward modelling. In: Curtis, A., Wood, R. (eds.), Geological Prior Information: Informing Science and Engineering. Geological Society Special Publication 239, 147-156.